Russian Journal of Earth Sciences Online ISSN: 1681-1208

Thermo-Tectonic Control on Conductive Heat Flow in a Moderate Heat-Flow Foreland Basin: Insights from the Upper Assam Basin, India

M. Gogoi[1,*], D. Bhuyan[1], and D. Majumdar[1]

[1] Department of Applied Geology, Dibrugarh University, Dibrugarh, Assam, India
* **Correspondence to:** Monmohan Gogoi, rs_monmohangogoi@dibru.ac.in

Abstract: Moderate heat-flow sedimentary basins are increasingly considered viable geothermal targets, particularly where mature hydrocarbon infrastructure reduces exploration risk. However, structural controls on conductive heat-flow distribution and associated uncertainty remain insufficiently quantified in foreland settings. This study develops an uncertainty-bounded thermo-tectonic framework for geothermal evaluation in the Upper Assam Basin, northeast India. Corrected bottom-hole temperature data from 34 deep wells are analysed using multiple empirical correction methods to construct a P10–P50–P90 temperature envelope, and conductive heat flow is calculated using depth-dependent harmonic bulk thermal conductivity accounting for lithologic layering. Statistical analysis and thermotomographic modelling are used to evaluate the relationship between basement architecture and thermal structure. Conductive heat flow ranges from ~41 to 108 mW m^{-2}, with most wells clustering between 60 and 75 mW m^{-2}, consistent with a moderate foreland geothermal regime. A statistically significant inverse relationship between basement depth and conductive heat flow (Pearson $r = -0.61$ to -0.66; Spearman $\rho = -0.71$; $p < 0.001$) suggests that sedimentary thermal blanketing exerts first-order control on basin-scale heat distribution. Reservoir temperatures of 120–170 °C at depths of 3.4–4.6 km support screening-level geothermal development using binary-cycle technologies. The study formalizes a foreland oilfield geothermal play model that links basement geometry, sediment thickness, reservoir architecture, and structural permeability to geothermal prospectivity. This framework extends geothermal evaluation beyond local resource appraisal and provides a transferable methodology for screening moderate heat-flow foreland basins worldwide.

Keywords: foreland basin geothermal, conductive heat flow, basement depth control, thermal blanketing, BHT correction uncertainty, oilfield-to-geothermal transition, ORC, Upper Assam Basin

Citation: Gogoi M., Bhuyan D., and Majumdar D. (2026), Thermo-Tectonic Control on Conductive Heat Flow in a Moderate Heat-Flow Foreland Basin, *Russian Journal of Earth Sciences*, 26, ES4007, EDN: CKURJJ, https://doi.org/10.2205/2026es001145

Review

Received: March 6, 2026
Accepted: June 29, 2026
Published: November 2, 2026

Copyright: © 2026. The Authors. This article is an open access article distributed under the terms and conditions of the Creative Commons Attribution (CC BY) license (https://creativecommons.org/licenses/by/4.0/).

1. Introduction

The global transition toward low-carbon energy systems has renewed interest in geothermal energy as a stable, dispatchable, and low-emission resource. Although high-enthalpy volcanic systems dominate current electricity production, moderate heat-flow sedimentary basins are increasingly recognized as viable targets for binary cycle and direct-use applications [*DiPippo*, 2016; *Quoilin et al.*, 2013]. In these settings, repurposing mature hydrocarbon fields offers a strategic advantage by leveraging existing infrastructure and reservoir characterization, thereby reducing exploration risk and capital expenditure [*Gautam et al.*, 2025; *Higgins and Pratson*, 2026; *Meenakshisundaram et al.*, 2024; *Nibbs et al.*, 2026; *Nordquist and Johnson*, 2012; *Ojaghi et al.*, 2025; *Xin et al.*, 2012].

Experience from intraplate provinces demonstrates that economically viable geothermal systems can develop in the absence of active magmatism. Structurally controlled reservoirs in the Basin-and-Range Province and fractured basement systems of the Upper

Rhine Graben show that moderate crustal heat flow, combined with permeability architecture, can sustain commercial production [*Dezayes and Lerouge*, 2019; *Faulds et al.*, 2016; *Simmons et al.*, 2018]. These examples underscore the role of structural segmentation and sedimentary thickness in governing subsurface thermal regimes.

In India, geothermal exploration has traditionally focused on high-enthalpy provinces such as Puga, Tatapani, and Manikaran [*Sarolkar*, 2018]. However, sedimentary basins characterized by moderate geothermal gradients are emerging as potential low-enthalpy resources. Feasibility studies in the Cambay Basin demonstrate the technical viability of Organic Rankine Cycle (ORC) systems within hydrocarbon fields [*Dalsania et al.*, 2024]. Despite over a century of petroleum exploration, the Upper Assam Basin remains comparatively under-evaluated for geothermal development, even though reported Paleogene reservoir temperatures of 90–150 °C fall within the operating range of binary power systems and direct-use applications [*Dutta et al.*, 2024; *Majumdar and Devi*, 2021].

The Upper Assam Basin is a tectonically complex foreland system formed by oblique convergence and underthrusting of the Indian Plate beneath the Eurasian and Burmese plates. Flexural subsidence, basement relief, and strike-slip reactivation generate pronounced lateral variation in sediment thickness and structural segmentation. Regional terrestrial heat flow (51–70 mW m^{-2}; mean ≈ 61 mW m^{-2}) places the basin within a moderate heat-flow regime [*Dutta et al.*, 2024; *Majumdar and Devi*, 2021]. In such foreland settings, basement geometry modulates conductive heat transfer through thermal blanketing, while faults and thrust systems may locally influence temperature distribution through permeability contrasts [*Angelier and Baruah*, 2009; *Hochstein et al.*, 2013]. However, the quantitative coupling between basement configuration, structural architecture, and conductive heat flow in the Upper Assam Basin has not been systematically evaluated.

Previous assessments primarily rely on corrected bottom-hole temperatures (BHT) to estimate geothermal gradients [*Dutta et al.*, 2024; *Majumdar and Devi*, 2021]. Although these studies confirm the presence of low- to medium-enthalpy resources, they do not rigorously quantify uncertainty associated with BHT correction methods nor explicitly resolve the mechanistic linkage between basement geometry and heat-flow distribution. As a result, spatial variability in geothermal prospectivity remains poorly constrained within a thermo-tectonic framework.

Despite extensive hydrocarbon exploration, the geothermal potential of the Upper Assam Basin remains poorly constrained, particularly with respect to the thermo-tectonic controls governing conductive heat flow and reservoir temperature distribution. This study aims to quantify the relationships among basement architecture, conductive heat flow, and geothermal prospectivity using corrected bottom-hole temperature data from 34 deep wells. An uncertainty-bounded thermal framework is developed through multiple BHT correction methods, conductive heat-flow modelling, statistical thermo-tectonic analysis, and thermotomographic reconstruction. The resulting assessment provides a process-based framework for evaluating geothermal resources in moderate heat-flow foreland basins and establishes a transferable thermo-tectonic model for geothermal exploration beyond the Upper Assam Basin.

2. Geological Setting

The Upper Assam Basin is a foreland basin situated between the Eastern Himalaya to the north and the Indo–Myanmar ranges to the south and southeast [*Nandy*, 2017]. It is developed through flexural subsidence related to India–Eurasia convergence and subsequent basement-involved deformation, resulting in pronounced lateral variations in sediment thickness, basement relief, and structural segmentation. The basin is bounded by the Himalayan foredeep to the north, the Mishmi crystalline complex to the northeast, the Naga–Patkai fold belt to the south and southeast, and the Shillong–Mikir Massifs to the west. Major structural elements include the Main Boundary Thrust (MBT), Main Frontal Thrust (MFT), the Naga Thrust system, and numerous NE–SW and E–W trending basement faults [*Nandy*, 2017]. These structures define the basin architecture and influence

permeability distribution, locally promoting or restricting fluid circulation within the geothermal system. The regional tectonic framework and distribution of analysed wells are shown in Figure 1.

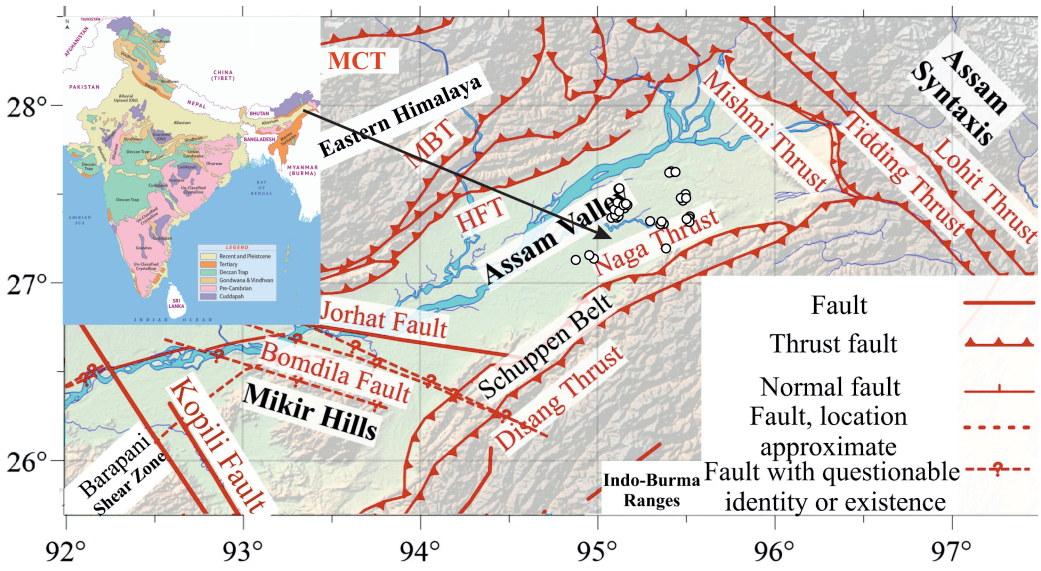


Figure 1. Tectonic framework of the Upper Assam Basin showing the location of 34 oil wells used for thermal analysis. Major thrust systems (MCT, MBT, Mishmi, Naga and Disang thrusts) define the foreland flexural architecture. Well distribution (white circle) illustrates clustering along structurally segmented corridors within the Assam Valley.

Stratigraphically, the basin comprises a Precambrian crystalline basement unconformably overlain by Cretaceous to Quaternary sedimentary successions. The Paleogene sequence—particularly the Eocene Jaintia Group and the overlying Oligocene Barail Group—hosts both the principal hydrocarbon reservoirs and the most prospective geothermal intervals. A compressed stratigraphic framework summarizing formation hierarchy, maximum thickness, and dominant lithology is presented in Table 1.

Within this succession, the Lakadong–Therria Formation occurs at depths of approximately 3.4–4.6 km and consists of alternating quartzitic sandstones, shales, and minor fossiliferous limestones, with thickness typically ranging between ~100–150 m in producing wells [*Bharali and Gogoi*, 2011; *Dutta et al.*, 2024; *Majumdar and Devi*, 2021]. Its burial depth, established reservoir quality, and lateral continuity make it the primary target for geothermal retrofitting. A representative composite wireline log illustrating Paleogene reservoir architecture and shale–sandstone alternations at geothermal depths is presented in Figure 2.

3. Materials and Methods

3.1. Dataset and BHT Corrections

Bottom-hole temperature (BHT) data from 34 deep oil wells penetrating the Paleogene sequence of the Upper Assam Basin are analysed. True vertical depths (TVD) range between ~3.0–4.8 km, with measured BHT values between 71–130 °C. A mean annual surface temperature of 26 °C is considered for all calculations based on regional climatological averages. Geothermal gradients are calculated using corrected BHT and corresponding TVDs. Since drilling operations disturb the thermal equilibrium of the borehole environment, measured BHT values commonly underestimate formation temperatures. To account for this effect, six empirical correction methods are evaluated: Harrison, Kehle, Förster, Modified Förster, Crowell, and Waples. These methods differ in their treatment of thermal recovery following drilling and shut-in periods [*Crowell*, 2011; *Förster and*

Table 1. Stratigraphic framework of the Upper Assam Basin showing major Paleogene formations and members, their maximum reported thicknesses, and generalized lithological characteristics. The Lakadong–Therria and associated units constitute the principal deep arenaceous reservoir interval evaluated for geothermal potential

Era	Period	Epoch	Group	Formation/Member		Maximum Thickness	Lithology
Cenozoic	Paleogene	Upper Eocene-Oligocene	Barail Group	Arenaceous Unit		1200 m, [*Hazarika et al.*, 2025]	Fine–medium grained sandstone with coal partings and carbonaceous shale [*Kumar et al.*, 2001].
		Eocene	Jaintia Group	Kopili Formation		552.5 m, [*Bhuyan*, 2016]	Alternating shale and sandstone with thin limestone and marl; black to grey splintery shale [*Bhuyan and Dutta*, 2015].
				Sylhet Formation	Prang Member	85.5 m, [*Bhuyan*, 2016]	Fossiliferous limestone with grey to bluish shale; minor calcareous/glauconitic sandstone [*Borgohain et al.*, 1998].
					Nurpuh Member	100 m, [*Das*, 2018]	Dark grey splintery shale with fine calcareous sandstone; minor glauconitic sandstone and limestone streaks [*Borgohain et al.*, 1998].
					Lakadong + Therria (Lk + Th)	151 m, [*Bharali and Gogoi*, 2011; *Majumdar and Devi*, 2021]	Alternating fine sandstone and splintery shale; glauconitic and fossiliferous limestone bands [*Borgohain et al.*, 1998].
		Palaeocene		Langpar Formation		50 m, [*Bharali and Gogoi*, 2011; *Deb and Barua*, 2010]	Shale with thin limestone and argillaceous sandstone bands [*Krishnan*, 1960].
Unconformity							
Precambrian			Basal Sandstone Basement Complex				Crystalline metamorphic rocks (gneiss, granite) [*Bhandari et al.*, 1973; *Nandy*, 1980, 1983, 2017].

Merriam, 1995; *Kehle et al.*, 1970; *Prater et al.*, 1981; *Waples and Ramly*, 2001]. Inter-method comparison indicates strong linear correlation among corrected temperatures ($r > 0.90$ in most pairwise comparisons), indicating robust relative ranking of wells despite absolute temperature differences. Förster-based corrections consistently produce higher gradients, while Kehle corrections produce more conservative estimates. Waples corrections generally occupy an intermediate position. The resulting bounded temperature range for each well is illustrated in Figure 3. The complete well-by-well corrected BHT dataset used to construct the uncertainty envelope is provided in Table A1 (Appendix A).

3.2. Thermal Uncertainty Envelope

To explicitly incorporate uncertainty associated with BHT correction methodology, a P10–P50–P90 thermal envelope is constructed for each well. The Kehle correction is considered as the conservative lower-bound estimate (P10), the Waples correction as the best-estimate scenario (P50), and the Förster correction as the upper-bound estimate (P90). Corrected geothermal gradients are calculated using $G = \frac{T_c - T_s}{\mathrm{TVD}}$, where G is the geothermal gradient (°C m^{-1} or K m^{-1}), T_c is the corrected bottom-hole temperature (°C or K), T_s is the mean annual surface temperature (26 °C), and TVD is the true vertical depth (m). The resulting gradient distributions are propagated through the conductive heat-flow calculations to generate uncertainty-bounded thermal and heat-flow estimates. This approach avoids reliance on a single correction model and permits assessment of methodological uncertainty throughout the analysis.

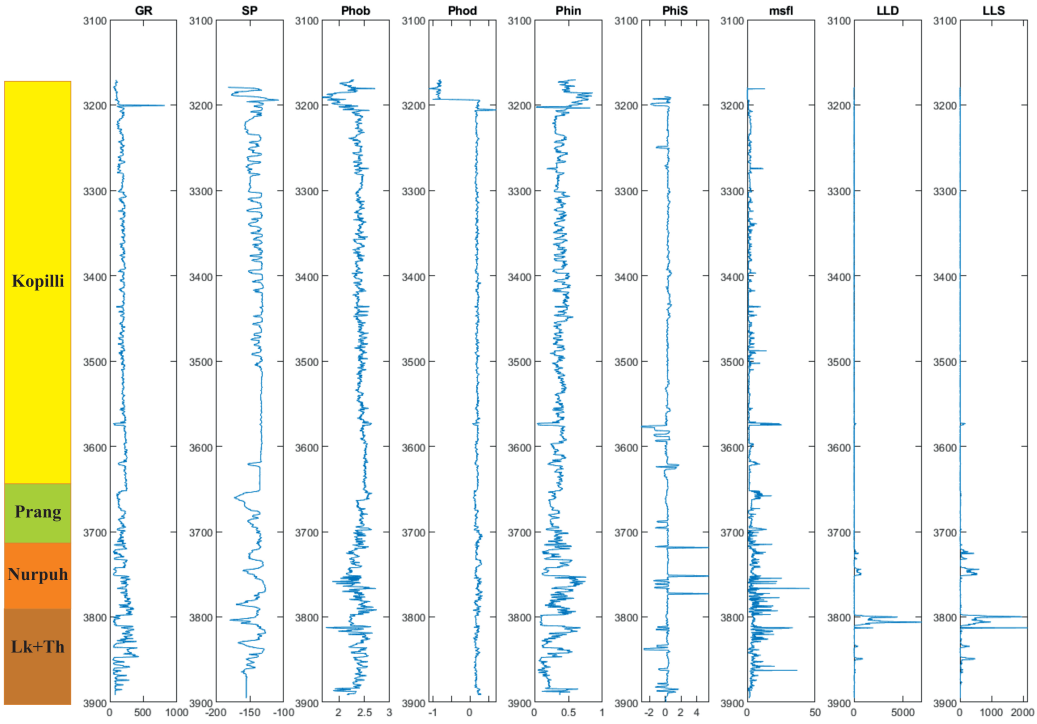


Figure 2. Representative well log (Well E) from the Upper Assam Basin. Composite wireline logs (GR, SP, density, neutron, and resistivity) from a deep oilfield well penetrating Paleogene stratigraphy (Kopili–Prang–Nurpur–Lakadong–Therria).

3.3. Conductive Heat-Flow Model

Conductive heat flow is calculated using Fourier's law using $q = k_{\text{bulk}}\, G$, where q is conductive heat flow (W m^{-2}), k_{bulk} is effective bulk thermal conductivity (W m^{-1} K^{-1}), and G is geothermal gradient (°C m^{-1} or K m^{-1}). To account for lithologic heterogeneity, bulk thermal conductivity is calculated using harmonic averaging across stratigraphic units $k_{\text{bulk}} = \frac{H}{\sum(h_i/k_i)}$; where h_i and k_i represent the thickness and thermal conductivity of individual lithologic layers within total thickness H. Thermal conductivity values assigned to major lithologies are based on published measurements and representative matrix properties: sandstone (2.8 W m^{-1} K^{-1}), shale (1.9 W m^{-1} K^{-1}), limestone (2.4 W m^{-1} K^{-1}), and crystalline basement (3.2 W m^{-1} K^{-1}) [*Bhuyan et al.*, 2022; *Devi et al.*, 2021; *Gascuel et al.*, 2020; *Gogoi et al.*, 2023; *Taye and Bhattacharyya*, 2013; *Tiwari et al.*, 2024; *Wandrey*, 2004; *Ye et al.*, 2022]. The full dataset of P10, P50, and P90 conductive heat-flow estimates for all 34 wells is reported in Table A2 (Appendix A).

At depths greater than approximately 3 km, porosity reduction associated with compaction is assumed to result in matrix-dominated thermal behaviour. As a result, fluid-related conductivity corrections are not incorporated. Harmonic conductivity values are calculated for each well based on stratigraphic composition and subsequently combined with corrected geothermal gradients to estimate conductive heat flow under P10, P50, and P90 scenarios.

3.4. Statistical Analysis

The relationship between conductive heat flow and basement depth is evaluated using both parametric and non-parametric statistical methods. Linear regression analysis is applied to quantify the dependence of heat flow on basement depth and to estimate regression slopes and coefficients of determination (R^2). Pearson correlation coefficients are calculated to assess linear association between variables, while Spearman rank correlation coefficients are used to evaluate monotonic relationships independent of distributional

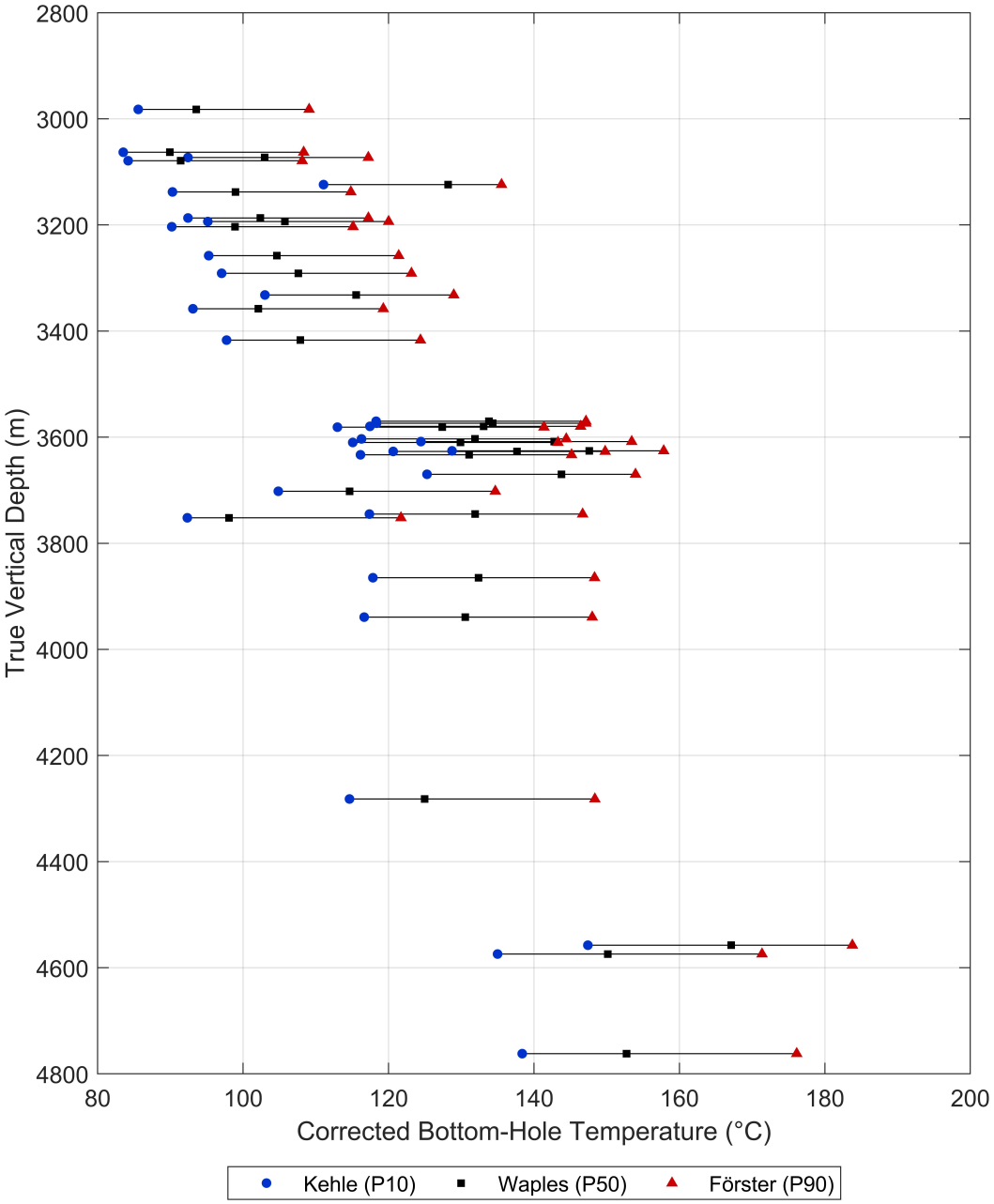


Figure 3. Corrected bottom-hole temperatures (BHT) for 34 wells using Kehle (P10), Waples (P50), and Förster (P90) methods. Horizontal bars denote the uncertainty range between conservative and upper-bound corrections at each true vertical depth.

assumptions. Statistical significance is evaluated using a significance threshold of $p < 0.05$. To assess the robustness of observed thermo-tectonic relationships, all analyses are carried out for the P10, P50, and P90 scenarios derived from the thermal uncertainty envelope.

3.5. Thermotomographic Modelling

Three-dimensional thermotomographic modelling is conducted using corrected BHTs, geothermal gradients, reservoir depths, and well coordinates from the 34 analysed wells. Spatial interpolation is carried out using a natural-neighbour interpolation scheme to generate continuous temperature fields across the study area [*Kiryukhin*, 1993]. Interpolated temperature grids are used to construct basin-wide temperature distribution maps, depth slices, and three-dimensional thermal volumes. Basement depth information derived from well-constrained basement picks is incorporated to evaluate spatial relationships

between basement relief and subsurface temperature distribution. The resulting thermotomographic model provides a spatial framework for analysing thermal variability within the Upper Assam Basin and for assessing the relationship between basement architecture and conductive heat-flow distribution.

3.6. Recoverable Thermal Energy and ORC Power Estimation

Recoverable geothermal energy is estimated using a simplified volumetric heat-in-place (HIP) approach. The theoretical thermal energy content, Q_{th} (J) of the reservoir is calculated using $Q_{\text{th}} = \rho_r c_r V(T_r - T_{\text{reinjection}})$, where ρ_r is bulk rock density (kg m^{-3}), c_r is specific heat capacity (J kg^{-1} K^{-1}), V is effective reservoir volume (m^3), T_r is reservoir temperature (°C or K) and $T_{\text{reinjection}}$ is reinjection temperature (°C or K). Reservoir temperatures used for HIP and Organic Rankine Cycle (ORC) screening calculations are taken from the P50 (Waples-corrected) thermal scenario and assumed to represent formation equilibrium temperatures. Reinjection temperatures between 35 and 50 °C are considered consistent with low-enthalpy binary geothermal systems. Since reservoir geometry, sweep efficiency, and long-term production behaviour remain uncertain, a conservative recovery-factor approach is considered. Effective reservoir thicknesses of 80–150 m and effective porosity values between 8–15 % are considered based on well log analysis. Recovery factors of 10–20 % are used, representing typical sandstone-hosted geothermal reservoirs in moderate heat-flow sedimentary basins.

Potential electrical generation is evaluated using ORC conversion efficiencies appropriate for low- to moderate-temperature geothermal resources [*Quoilin et al.*, 2013]. Electrical power output is estimated using $P_e = \eta_{\text{ORC}}\, Q_{\text{rec}}$, where P_e is electrical power output, η_{ORC} is the ORC conversion efficiency, and Q_{rec} is the recoverable thermal power ($Q_{\text{rec}} = RF \times Q_{\text{th}}$, RF is the recovery factor). Since practical ORC systems operate below the theoretical thermodynamic efficiency, three performance scenarios corresponding to 25 %, 40 %, and 60 % of the theoretical efficiency are evaluated within P50 thermal scenario. The complete well-by-well calculations are provided in Table A3 (Appendix A). The resulting estimates represent screening-level single-well geothermal potential rather than basin-wide in-place resources. They are intended to provide a first-order assessment of geothermal feasibility and should not be interpreted as production forecasts.

4. Results

4.1. Conductive Heat-Flow Distribution

Conductive heat-flow estimates derived from the P10–P50–P90 uncertainty envelope indicate a moderate regional thermal regime across the Upper Assam Basin. Under P10 conditions, heat flow ranges from 41–86 mW m^{-2} (mean 54.7 mW m^{-2}), whereas P50 estimates range from 42–82 mW m^{-2} (mean 66.4 mW m^{-2}). The P90 scenario yields values between 58 and 108 mW m^{-2} (mean 74.3 mW m^{-2}). Most wells cluster within the 50–75 mW m^{-2} interval under P50 conditions (Figure 4).

4.2. Basement Depth versus Conductive Heat Flow

Basement depth varies from approximately 4.3 to 5.6 km across the study area. Linear regression indicates a statistically significant inverse relationship between basement depth and conductive heat flow across the uncertainty envelope. Regression slopes vary between −14.36 and −19.19 mW m^{-2} km^{-1}, with R^2 values of 0.37–0.43 ($p < 0.001$). The consistent negative slopes across conservative (P10), median (P50), and upper-bound (P90) heat-flow estimates suggest that structural control on the basin thermal regime is robust and not a correction artifact. Pearson correlation coefficients range from −0.61 to −0.66, while the Spearman rank correlation coefficient for the P50 dataset is −0.71 (Figure 5; Table 2).

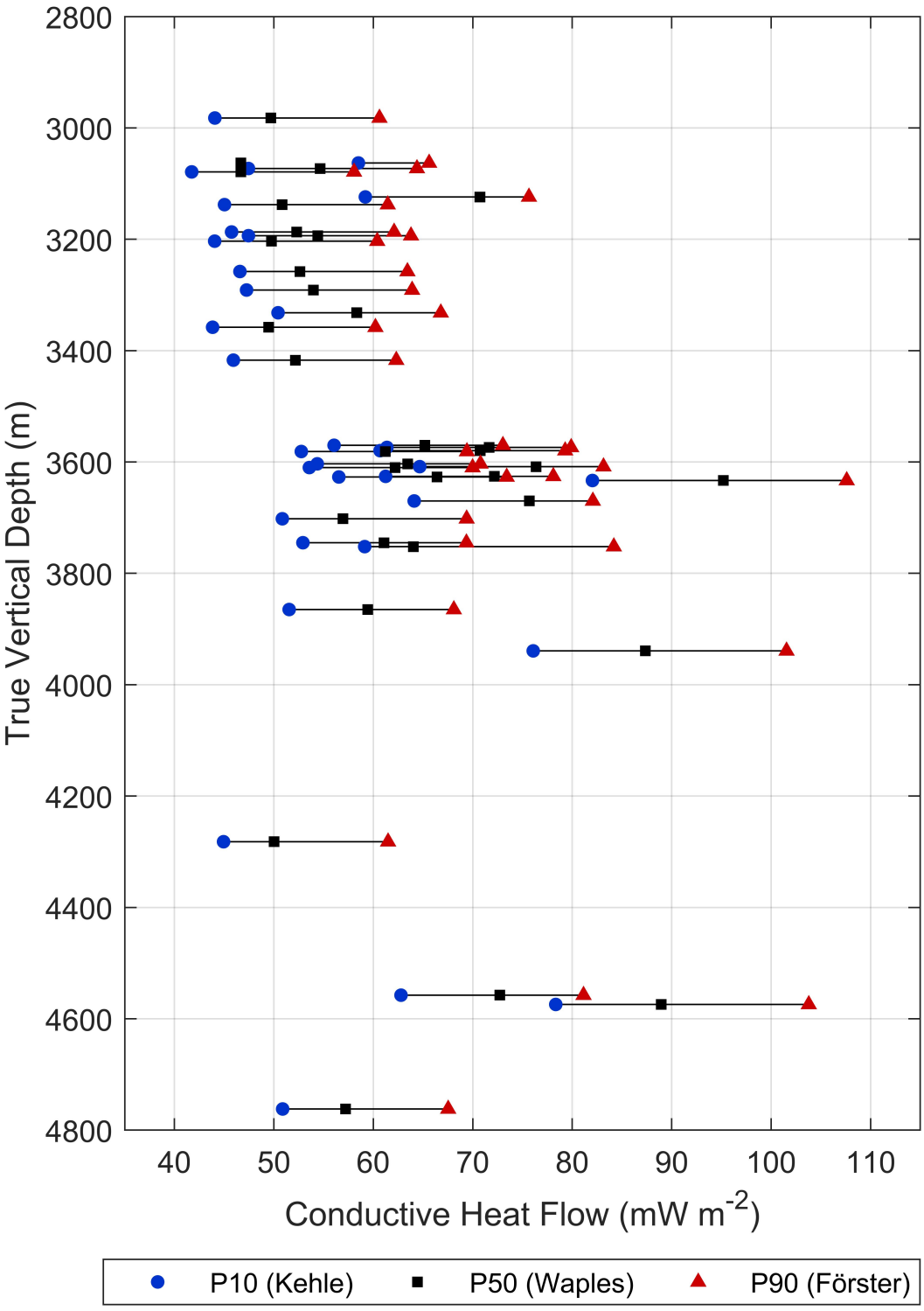


Figure 4. Conductive heat flow estimates for 34 wells derived using Kehle (P10, conservative), Waples (P50, best estimate), and Förster (P90, upper bound) correction methods. Horizontal bars represent the method-dependent uncertainty range at each true vertical depth.

4.3. Structural Influence on Geothermal Gradients

Regression analysis of gradient versus distance to major thrust structures indicates localized enhancement of geothermal gradients in structurally segmented zones. Although the correlation is weaker than that observed for basement depth, wells situated closer to major thrusts tend to show slightly elevated gradients relative to basin averages. This pattern

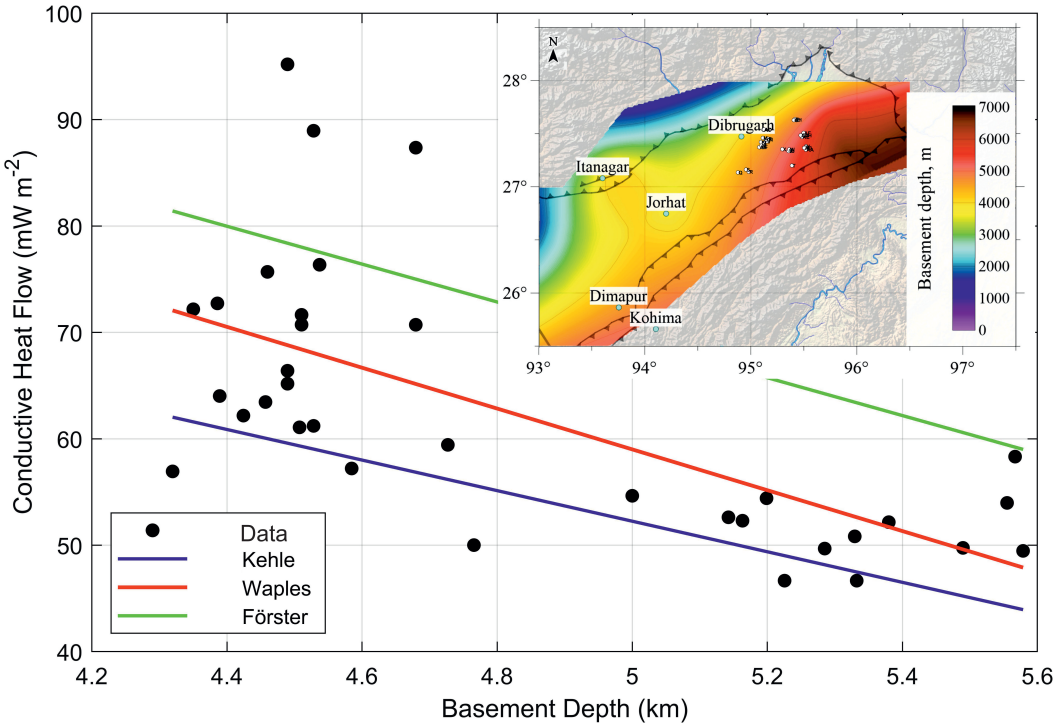


Figure 5. Method-independent regression stability between basement depth and conductive heat flow.

Table 2. Statistical summary of conductive heat-flow estimates derived from P10 (Kehle), P50 (Waples), and P90 (Förster) bottom-hole temperature correction scenarios. The table reports mean heat flow, standard deviation (SD), coefficient of variation (CV), and regression statistics for the relationship between basement depth and heat flow, including slope, coefficient of determination (R^2), Pearson's r, and Spearman's rank correlation (ρ)

Parameter	P10 (Kehle)	P50 (Waples)	P90 (Förster)
Mean Heat Flow (mW m^{-2})	54.7	66.4	74.3
Standard Deviation (mW m^{-2})	11.2	14.6	16.8
Coefficient of Variation (CV)	0.20	0.22	0.23
Regression Slope (mW m^{-2} km^{-1})	−14.36	−19.19	−17.79
R^2 (Basement Depth vs Heat Flow)	0.37	0.43	0.37
Pearson's r	−0.61	−0.66	−0.61
p-value (slope)	< 0.001	< 0.001	< 0.001
Spearman ρ (P50 only)	—	−0.71	—

suggests that structural discontinuities may facilitate limited advective heat redistribution through enhanced fracture permeability.

4.4. Conductive versus Advective Heat Transport

Order-of-magnitude Peclet ($Pe = \frac{\rho c v L}{k} \approx 1$–$15$) and Rayleigh number ($Ra = \frac{g\beta\Delta T k H}{\nu\alpha} \approx 10$–$500$) estimates (Table A4, Appendix A), together with the observed reservoir permeability characteristics, suggest that heat transport within the Upper Assam Basin is predominantly conductive at the basin scale. Basin-scale hydrothermal convection is unlikely within the Lakadong–Therria reservoir system. Nevertheless, localized fault-controlled fluid circulation may occur within structurally favourable sectors and contribute to secondary advective heat transport.

4.5. Thermotomographic Model

Three-dimensional thermotomographic modelling reveals pronounced lateral temperature variability across the basin (Figure 6). Interpolated P50 temperatures exceed 150 °C in the western and southwestern sectors, whereas northeastern sectors generally remain below 110 °C. The 4500 m depth slice identifies several localized thermal highs. Basement depth mapping indicates spatial coincidence between elevated temperatures and relatively shallow basement domains. The 3-D temperature volume further shows the persistence of coherent thermal anomalies between approximately 4 and 5.5 km depth. The model reveals systematic correspondence between elevated temperatures and shallower basement domains, supporting the interpretation that basement geometry and sedimentary thermal blanketing exert first-order controls on conductive heat flow and geothermal prospectivity within the basin.

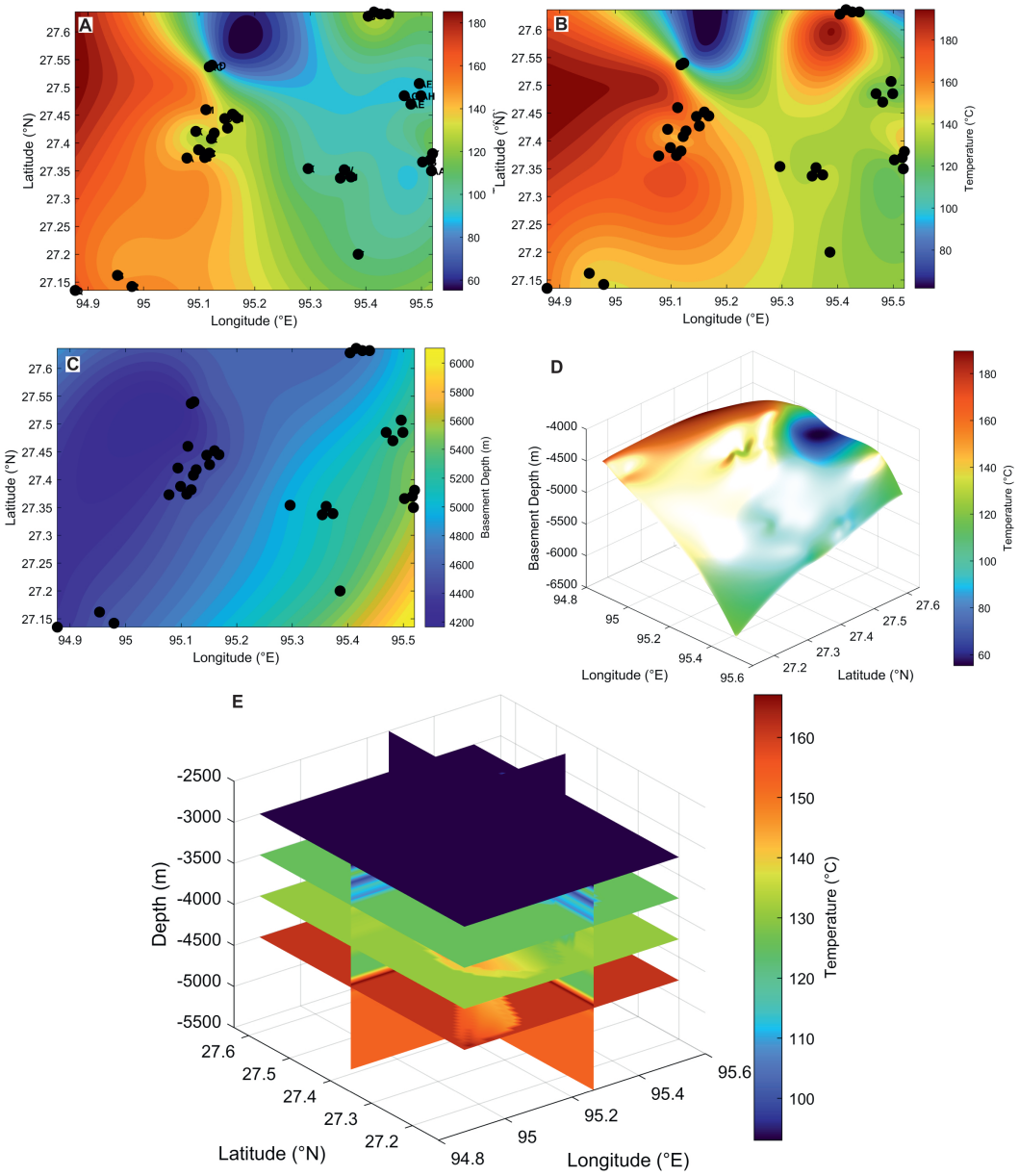


Figure 6. Integrated thermotomographic model of the Upper Assam Basin. (*A*) Interpolated P50 temperature distribution from 34 geothermal wells. (*B*) Predicted temperature field at 4500 m depth. (*C*) Basement depth distribution derived from well-constrained basement picks. (*D*) Thermo-tectonic basement surface. (*E*) 3-D thermotomographic temperature volume.

4.6. Reservoir Properties and Geothermal Resource Potential

Effective porosity within the Lakadong–Therria reservoir ranges from 9.1 % (P10) to 24.7 % (P90), with permeability estimates ranging from 0.56 to 170.26 mD (Table 3). Under P50 conditions, reservoir temperatures range between 120 and 170 °C at depths of 3.4–4.6 km. Under the P50 thermal scenario, estimated gross electrical outputs span approximately 36–144 kW for the 25 % efficiency case, 57–230 kW for the 40 % case, and 86–345 kW for the 60 % case. The complete well-by-well ORC power estimates under the P50 thermal scenario are provided in Table A3 (Appendix A). The highest power potentials occur in wells Q, R, and S, which correspond to the highest predicted reservoir temperatures within the dataset.

Table 3. Reservoir properties of the Lakadong–Therria geothermal interval

Parameter	P10	P50	P90
Effective porosity, Φ_e	0.091	0.170	0.247
Water saturation, S_w	0.204	0.411	0.654
R_t (Ω·m)	20.972	244.59	3995.922
Permeability (mD)	0.56	68.56	170.26

5. Discussion

5.1. Basement Geometry as the Primary Control on Conductive Heat Flow

The statistically significant inverse relationship between basement depth and conductive heat flow suggests that basement architecture exerts a first-order control on the thermal structure of the Upper Assam Basin. Pearson correlation coefficients between −0.61 and −0.66 and a Spearman rank coefficient of −0.71 indicate that the observed relationship is both robust and independent of the specific BHT correction methodology employed. The persistence of this trend across the P10–P50–P90 uncertainty envelope suggests that the thermo-tectonic signal is geological rather than methodological in origin.

The physical mechanism responsible for this relationship is sedimentary thermal blanketing. In foreland basins, increasing sediment thickness increases the thermal resistance between the basement and the surface, thereby attenuating conductive heat transfer. As a result, deep depocentres show lower conductive heat flow, whereas basement highs concentrate conductive flux by reducing the thickness of insulating sedimentary cover. Similar thermal blanketing effects have been documented in several foreland and intracratonic basins worldwide, where basement relief exerts a measurable influence on regional geothermal gradients. Unlike volcanic geothermal systems where heat anomalies are commonly associated with magmatic intrusions, the Upper Assam Basin indicates that significant thermal heterogeneity may develop solely through geometric modification of conductive heat transport.

5.2. Structural Permeability and Localized Thermal Enhancement

Although basement depth explains most of the observed thermal variability, structural segmentation appears to exert a secondary influence on geothermal gradients. Wells located near major thrust systems and basement-rooted faults commonly show slightly elevated thermal gradients relative to basin averages. The effect is considerably weaker than the basement-depth control, indicating that faults do not fundamentally alter the regional thermal regime. However, structural discontinuities may enhance fracture permeability and facilitate localized fluid circulation. Such behaviour has been reported in numerous sedimentary geothermal systems where fault zones act as preferential pathways for heat and fluid migration. Therefore, the available evidence supports a hierarchical thermo-tectonic framework in which basement geometry establishes the regional conductive thermal field,

whereas structural permeability locally modifies reservoir temperatures and geothermal productivity.

5.3. Conductive versus Advective Heat Transport

Order-of-magnitude Peclet (1–15) and Rayleigh (10–500) number estimates indicate that basin-scale hydrothermal convection is unlikely within the Lakadong–Therria reservoir system. Estimated values remain below thresholds typically associated with sustained hydrothermal convection, suggesting that large-scale buoyancy-driven circulation is unlikely within the Upper Assam Basin. However, the Lakadong–Therria reservoir interval retains moderate porosity and permeability despite burial depths exceeding 3 km. Combined with the presence of basement-rooted faults and fracture systems, these reservoir characteristics indicate that localized advective heat transport cannot be entirely excluded. Therefore, the geothermal regime of the basin is best interpreted as dominantly conductive with localized fault-controlled advective enhancement. Under such conditions, conductive models likely provide conservative estimates of geothermal potential because localized fluid circulation may increase reservoir temperatures beyond those predicted by purely conductive heat transfer.

5.4. Implications of the Thermotomographic Model

The thermotomographic model provides independent spatial evidence supporting the thermo-tectonic relationships identified through statistical analysis. Elevated temperature domains identified in the western and southwestern sectors coincide with relatively shallow basement regions, whereas cooler zones generally correspond to deeper structural compartments. The spatial correspondence between temperature anomalies and basement relief strengthens the interpretation that basement geometry exerts first-order control on conductive heat flow. The persistence of coherent thermal bodies within the three-dimensional temperature volume further suggests that these anomalies represent basin-scale thermal domains rather than interpolation artefacts associated with individual wells. From an exploration perspective, the thermotomographic model provides a practical framework for identifying favourable geothermal targets by integrating thermal, structural, and reservoir information within a single spatial model.

5.5. Implications for Geothermal Resource Development

The estimated reservoir temperatures of 120–170 °C and predicted ORC outputs of approximately 100–300 kW per well indicate that the Upper Assam Basin possesses technically viable geothermal resources despite its moderate regional heat flow. Rather than constituting a single high-enthalpy geothermal field, the basin is better interpreted as a distributed geothermal system composed of multiple structurally compartmentalized reservoirs. Such systems may be particularly attractive for oilfield-to-geothermal transition strategies because existing hydrocarbon infrastructure substantially reduces exploration and development costs. Therefore, the results suggest that moderate heat-flow foreland basins should not be excluded from geothermal evaluation solely because they lack active magmatism.

5.6. Transferability to Other Foreland Basins

Although developed using the Upper Assam Basin as a case study, the thermo-tectonic relationships identified here are potentially applicable to many foreland and intermontane basins worldwide. The key geological requirements include moderate regional conductive heat flow (50–90 mW m^{-2}), significant lateral variability in basement depth, sedimentary thickness exceeding approximately 3 km, deep permeable sandstone reservoirs, structurally segmented permeability pathways, and mature hydrocarbon infrastructure. Where these conditions coexist, geothermal prospectivity may be controlled more strongly by basin geometry and thermal blanketing than by anomalous mantle heat input.

5.7. Limitations and Future Work

Several limitations should be acknowledged. First, the thermal framework relies on corrected BHT data rather than equilibrium temperature measurements. Second, permeability distributions are inferred from available reservoir data and have not been calibrated using dedicated geothermal production tests. Third, the thermotomographic model is constrained by the spatial distribution of available wells and therefore may not fully resolve smaller-scale thermal heterogeneities. Future work should incorporate transient thermal modelling, coupled thermo-hydraulic simulations, and dedicated geothermal reservoir testing to evaluate long-term production sustainability and reinjection performance.

5.8. Foreland Oilfield Geothermal Play Model

The integrated thermal, structural, and thermotomographic analyses conducted in this study provide the basis for proposing a '*foreland oilfield geothermal play model*' for the Upper Assam Basin (Figure 7). The results show that geothermal prospectivity within this moderate heat-flow foreland basin is controlled primarily by the interaction among basement architecture, sedimentary thermal blanketing, reservoir distribution, and structurally enhanced permeability rather than by anomalous mantle heat input. This mechanism differs fundamentally from conventional geothermal systems associated with volcanic arcs, rift environments, or magmatic provinces.

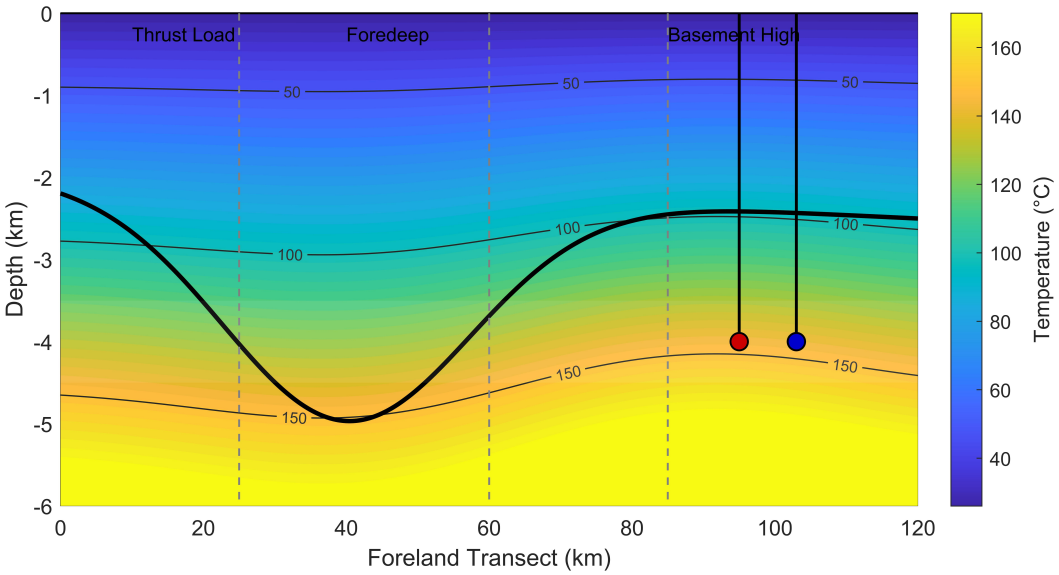


Figure 7. Quantitatively scaled conceptual model of the '*foreland oilfield geothermal play*' in the Upper Assam Basin.

The play model indicates that geothermal prospectivity is concentrated above basement highs where reduced sediment thickness enhances conductive heat transfer and elevates reservoir temperatures. Basement-rooted faults and thrust-related structures may locally enhance permeability and facilitate limited fluid circulation. These features are interpreted as controls on reservoir accessibility and productivity rather than primary heat sources. The Lakadong–Therria interval represents the principal geothermal target because it combines favourable reservoir properties with predicted temperatures of 120–170 °C at depths of 3.4–4.6 km. The regional geological cross-sections previously published by Lozovsky et al. [*Lozovsky et al.*, 2025] and Kumar and Sain [*Kumar and Sain*, 2022] are integrated with the thermo-tectonic framework developed in this study (Figure 8). The illustrated isotherms are schematic and represent the generalized thermal architecture inferred from the thermotomographic and heat-flow analyses.

The Foreland Oilfield Geothermal Play Model proposed here provides a process-based framework for evaluating geothermal potential in sedimentary basins characterized by

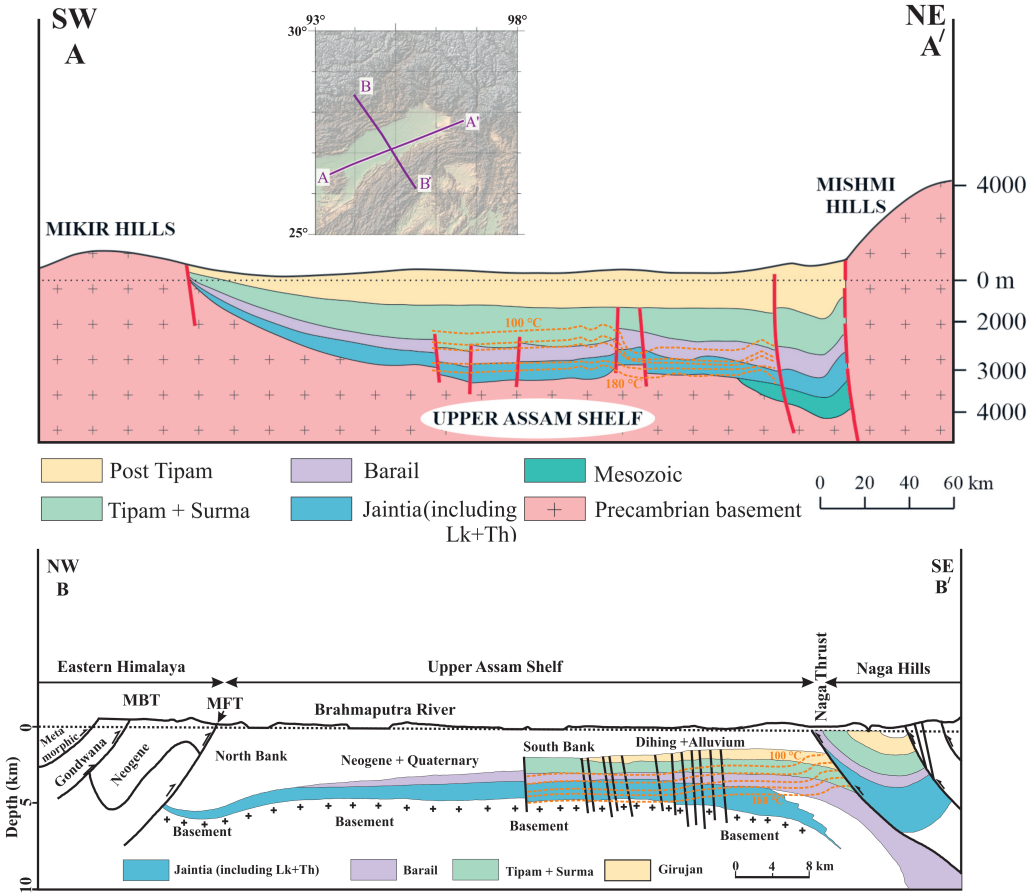


Figure 8. Conceptual geological–geothermal framework of the Upper Assam Basin showing the relationships among basement architecture, major fault systems, Lakadong–Therria reservoir intervals and inferred thermal anomalies. Geological cross-sections are modified from previously published regional interpretations of the basin [*Kumar and Sain*, 2022; *Lozovsky et al.*, 2025]. The illustrated isotherms are schematic and intended to represent generalized thermal architecture.

moderate regional heat flow, significant basement relief, deep permeable reservoirs, and mature hydrocarbon infrastructure. By formalizing the relationships among basement geometry, conductive heat transfer, structural permeability, and reservoir distribution, the model extends geothermal assessment beyond local feasibility studies and offers a transferable framework for screening geothermal resources in foreland basins worldwide.

6. Conclusions

This study shows that geothermal prospectivity in moderate heat-flow foreland basins is governed primarily by thermo-tectonic controls rather than by anomalous magmatic heat sources. The integrated analysis shows that basement geometry, sedimentary thermal blanketing, and structural permeability collectively regulate conductive heat-flow distribution and reservoir temperature within the Upper Assam Basin.

The persistence of the observed thermo-tectonic relationships across the P10–P50–P90 uncertainty envelope indicates that the identified structural controls are robust and not artifacts of bottom-hole temperature correction methodology. The results support the use of uncertainty-bounded conductive modelling as a reliable approach for geothermal assessment in mature sedimentary basins.

A principal contribution of this study is the development of the foreland oilfield geothermal play model, which provides a process-based framework linking basement relief, conductive heat transfer, reservoir distribution, and permeability architecture. The

model shows that economically relevant geothermal resources may occur in foreland basins lacking active magmatism when favourable structural and stratigraphic conditions coexist.

Beyond the Upper Assam Basin, the proposed framework offers a transferable methodology for identifying geothermal targets in hydrocarbon provinces undergoing energy transition and infrastructure repurposing. By integrating thermal uncertainty analysis with thermo-tectonic interpretation, the study advances geothermal evaluation from descriptive resource appraisal toward a predictive basin-scale exploration framework.

Acknowledgments. The authors gratefully acknowledge Oil India Limited (OIL) for providing access to the Bottom-Hole Temperature (BHT) data used in this study. The authors also acknowledge the support of faculty, colleagues and all those who assisted directly or indirectly in this research which is a part of the ongoing Ph.D. work of the first author. The authors are thankful to the anonymous reviewers for examining the manuscript, expressing critical comments, views and valuable suggestions on improving the quality of the paper.

Funding. This research was not financially supported by any agencies.

Data Availability. Processed datasets are provided in Supplementary Tables A1, A2, A3, and A4. Additional data are available from the corresponding author upon reasonable request.

Appendix A.

Table A1. Corrected bottom-hole temperatures (BHTs) and corresponding geothermal gradients for the 34 analyzed wells in the Upper Assam Basin. P10, P50, and P90 scenarios correspond to the Kehle, Waples, and Förster correction methods, respectively. Geothermal gradients (G) are reported in °C/100 m and were calculated using corrected BHT values and true vertical depth (TVD). The P10–P50–P90 envelope defines the uncertainty range used in subsequent conductive heat-flow modelling and geothermal resource assessment

No.	Well	TVD (m)	Raw BHT (°C)	P10 (Kehle) BHT (°C)	G (°C/100 m)	P50 (Waples) BHT (°C)	G (°C/100 m)	P90 (Förster) BHT (°C)	G (°C/100 m)
1	A	3670.00	111.00	125.29	2.79	143.77	3.29	153.96	3.57
2	B	3608.36	110.00	124.45	2.81	142.79	3.32	153.44	3.61
3	C	3573.80	104.00	118.35	2.67	134.33	3.12	147.14	3.47
4	D	3570.00	103.90	118.29	2.67	133.80	3.10	147.15	3.48
5	E	3864.96	102.70	117.85	2.45	132.38	2.83	148.33	3.24
6	F	3939.23	101.10	116.65	2.38	130.54	2.73	148.01	3.17
7	G	3123.99	98.80	111.06	2.82	128.20	3.37	135.54	3.60
8	H	4282.00	98.00	114.63	2.14	124.97	2.38	148.37	2.93
9	I	3626.92	106.11	120.64	2.69	137.67	3.16	149.79	3.50
10	J	3579.63	103.00	117.44	2.64	133.07	3.07	146.41	3.45
11	K	3610.00	101.00	115.08	2.55	129.89	2.96	143.30	3.33
12	L	3581.18	98.80	112.97	2.51	127.39	2.91	141.37	3.31
13	M	3625.80	114.22	128.73	2.92	147.61	3.44	157.84	3.72
14	N	3745.00	102.77	117.37	2.52	131.92	2.91	146.69	3.30
15	O	3603.30	102.22	116.28	2.59	131.88	3.02	144.44	3.37
16	P	3633.25	101.67	116.14	2.56	131.08	2.97	145.17	3.36
17	Q	4557.60	129.62	147.41	2.73	167.11	3.16	183.78	3.53
18	R	4762.00	120.00	138.38	2.42	152.73	2.72	176.13	3.22
19	S	4574.24	117.20	134.99	2.45	150.15	2.78	171.36	3.24
20	T	3417.10	84.40	97.73	2.19	107.88	2.48	124.39	2.97
21	U	3193.60	82.70	95.15	2.26	105.75	2.59	120.01	3.04

Continued on next page

Table A1. Corrected bottom-hole temperatures (BHTs) and corresponding geothermal gradients for the 34 analyzed wells in the Upper Assam Basin. P10, P50, and P90 scenarios correspond to the Kehle, Waples, and Förster correction methods, respectively. Geothermal gradients (*G*) are reported in °C/100 m and were calculated using corrected BHT values and true vertical depth (TVD). The P10–P50–P90 envelope defines the uncertainty range used in subsequent conductive heat-flow modelling and geothermal resource assessment(Continued)

22	V	3257.90	82.20	95.27	2.22	104.64	2.51	121.40	3.02
23	W	3186.90	80.00	92.42	2.18	102.37	2.49	117.23	2.96
24	X	3072.90	80.00	92.42	2.26	102.96	2.60	117.22	3.07
25	Y	3332.00	90.00	103.00	2.40	115.54	2.78	128.97	3.18
26	Z	3291.16	84.00	97.05	2.25	107.59	2.57	123.15	3.04
27	AA	3358.00	80.00	93.10	2.09	102.10	2.36	119.28	2.87
28	AB	3203.40	77.70	90.19	2.10	98.89	2.37	115.12	2.88
29	AC	3701.98	90.00	104.84	2.21	114.64	2.48	134.68	3.02
30	AD	3752.00	77.70	92.33	1.85	98.07	2.00	121.71	2.63
31	AE	3137.80	78.00	90.29	2.14	98.95	2.42	114.82	2.93
32	AF	2982.23	73.80	85.58	2.10	93.56	2.37	109.08	2.89
33	AG	3079.00	72.20	84.19	1.99	91.42	2.22	108.13	2.76
34	AH	3063.00	71.10	83.52	1.98	89.93	2.19	108.33	2.79

Table A2. Conductive heat-flow estimates (mW m^{-2}) calculated for the 34 analyzed wells using six empirical bottom-hole temperature correction methods. P10 (Kehle), P50 (Waples), and P90 (Förster) define the uncertainty-bounded heat-flow envelope used throughout this study. Heat-flow values are computed using corrected geothermal gradients and formation-specific harmonic bulk thermal conductivity estimates

Well	Harrison	Modified Förster	Crowell	P10 (Kehle)	P50 (Waples)	P90 (Förster)
A	67.022	90.076	88.572	64.108	75.687	82.074
B	67.555	91.411	89.760	64.664	76.355	83.145
C	64.331	88.157	86.567	61.366	71.649	79.894
D	58.746	80.606	79.135	56.051	65.176	73.029
E	53.665	75.633	73.775	51.534	59.431	68.095
F	78.915	113.257	110.080	76.077	87.359	101.551
G	62.887	82.481	82.474	59.195	70.717	75.648
H	45.961	69.253	66.688	44.938	50.009	61.483
I	59.122	80.979	79.428	56.531	66.394	73.413
J	63.597	87.608	85.963	60.678	70.723	79.291
K	56.355	77.246	76.001	53.565	62.180	69.982
L	55.535	76.801	75.481	52.757	61.214	69.411
M	63.835	85.650	84.115	61.235	72.172	78.098
N	55.394	76.744	75.191	52.919	61.077	69.360
O	57.166	78.037	76.801	54.361	63.455	70.776
P	86.012	119.043	116.753	82.032	95.192	107.603
Q	62.844	89.934	86.558	62.783	72.725	81.137
R	50.408	75.573	72.292	50.880	57.210	67.527
S	78.429	115.982	111.302	78.343	88.950	103.787
T	49.123	69.390	68.615	45.926	52.164	62.308
U	51.036	70.629	70.478	47.442	54.414	63.787
V	50.004	70.647	70.028	46.586	52.624	63.430
W	49.350	68.926	68.794	45.745	52.301	62.089
X	51.179	71.476	71.339	47.441	54.644	64.388

Continued on next page

Table A2. Conductive heat-flow estimates (mW m^{-2}) calculated for the 34 analyzed wells using six empirical bottom-hole temperature correction methods. P10 (Kehle), P50 (Waples), and P90 (Förster) define the uncertainty-bounded heat-flow envelope used throughout this study. Heat-flow values are computed using corrected geothermal gradients and formation-specific harmonic bulk thermal conductivity estimates(Continued)

Y	53.776	73.777	73.235	50.417	58.324	66.785
Z	50.640	71.030	70.437	47.252	53.975	63.900
AA	47.148	67.234	66.615	43.837	49.467	60.210
AB	47.623	67.247	67.063	44.045	49.749	60.392
AC	53.462	77.761	75.859	50.849	56.935	69.384
AD	62.874	95.437	93.058	59.130	64.021	84.184
AE	48.706	68.278	68.251	45.032	50.830	61.450
AF	47.949	67.354	67.734	44.064	49.684	60.616
AG	45.496	64.766	64.971	41.735	46.667	58.062
AH	41.494	65.475	45.889	58.500	46.667	65.612

Table A3. Screening-level Organic Rankine Cycle (ORC) power estimates for the 34 analyzed wells based on P50 (Waples) reservoir temperatures. Theoretical thermodynamic efficiency (η) is calculated from reservoir and working-fluid temperatures. Practical ORC performance scenarios are evaluated using 25 %, 40 %, and 60 % of the theoretical efficiency (η_{25}, η_{40}, and η_{60}, respectively). Power estimates represent gross electrical output prior to parasitic losses and should be regarded as indicative single-well screening estimates rather than production forecasts

Well	Reservoir Temp. (°C)	ΔT_{lm} (°C)	η	η_{25}	η_{40}	Power (25 % η) (kW)	Power (40 % η) (kW)	Power (60 % η) (kW)
A	143.77	31.911	0.2730	0.0682	0.1092	130.7	209.1	313.6
B	142.79	31.632	0.2713	0.0678	0.1085	128.7	205.9	308.9
C	134.33	29.187	0.2561	0.0640	0.1025	112.1	179.4	269.1
D	133.80	29.031	0.2552	0.0638	0.1021	111.1	177.8	266.7
E	132.38	28.613	0.2526	0.0631	0.1010	108.4	173.4	260.1
F	130.54	28.067	0.2491	0.0623	0.0997	104.9	167.8	251.7
G	128.20	27.366	0.2448	0.0612	0.0979	100.5	160.8	241.1
H	124.97	26.388	0.2386	0.0597	0.0955	94.5	151.1	226.7
I	137.67	30.161	0.2622	0.0655	0.1049	118.6	189.8	284.7
J	133.07	28.816	0.2538	0.0635	0.1015	109.7	175.5	263.3
K	129.89	27.873	0.2479	0.0620	0.0992	103.7	165.9	248.8
L	127.39	27.122	0.2432	0.0608	0.0973	99.0	158.3	237.5
M	147.61	32.995	0.2796	0.0699	0.1118	138.4	221.4	332.1
N	131.92	28.477	0.2517	0.0629	0.1007	107.5	172.0	258.0
O	131.88	28.465	0.2516	0.0629	0.1007	107.4	171.9	257.9
P	131.08	28.227	0.2501	0.0625	0.1001	105.9	169.5	254.2
Q	167.11	38.319	0.3115	0.0779	0.1246	179.1	286.5	429.8
R	152.73	34.420	0.2883	0.0721	0.1153	148.8	238.1	357.2
S	150.15	33.705	0.2839	0.0710	0.1136	143.6	229.7	344.5
T	107.88	20.934	0.2045	0.0511	0.0818	64.2	102.7	154.1
U	105.75	20.213	0.2000	0.0500	0.0800	60.6	97.0	145.5
V	104.64	19.832	0.1976	0.0494	0.0791	58.8	94.1	141.1
W	102.37	19.044	0.1928	0.0482	0.0771	55.1	88.1	132.2
X	102.96	19.250	0.1941	0.0485	0.0776	56.0	89.7	134.5
Y	115.54	23.443	0.2202	0.0550	0.0881	77.4	123.9	185.8
Z	107.59	20.836	0.2039	0.0510	0.0815	63.7	101.9	152.9

Continued on next page

Table A3. Screening-level Organic Rankine Cycle (ORC) power estimates for the 34 analyzed wells based on P50 (Waples) reservoir temperatures. Theoretical thermodynamic efficiency (η) is calculated from reservoir and working-fluid temperatures. Practical ORC performance scenarios are evaluated using 25 %, 40 %, and 60 % of the theoretical efficiency (η_{25}, η_{40}, and η_{60}, respectively). Power estimates represent gross electrical output prior to parasitic losses and should be regarded as indicative single-well screening estimates rather than production forecasts(Continued)

AA	102.10	18.949	0.1922	0.0481	0.0769	54.6	87.4	131.1
AB	98.89	17.806	0.1852	0.0463	0.0741	49.5	79.2	118.7
AC	114.64	23.154	0.2183	0.0546	0.0873	75.8	121.3	182.0
AD	98.07	17.508	0.1834	0.0459	0.0734	48.2	77.1	115.6
AE	98.95	17.827	0.1854	0.0463	0.0741	49.6	79.3	119.0
AF	93.56	15.823	0.1734	0.0433	0.0694	41.2	65.8	98.8
AG	91.42	14.992	0.1685	0.0421	0.0674	37.9	60.6	91.0
AH	89.93	14.399	0.1651	0.0413	0.0661	35.7	57.1	85.6

Table A4. Order-of-magnitude Peclet and Rayleigh number estimates for the Lakadong–Therria geothermal reservoir. Parameter values represent typical ranges inferred from reservoir properties and published thermo-hydraulic characteristics of deep sandstone reservoirs. Calculations are intended to assess the relative importance of conductive and advective heat transport at the basin scale

Parameter	Symbol	Assumed Range	Units
Reservoir thickness	H	100–150	m
Effective porosity	Φ_e	0.09–0.25	—
Permeability	k	0.56–170.26	mD
Fluid velocity	v	10^{-8}–10^{-7}	m s^{-1}
Thermal conductivity	λ	2.1–2.3	W m^{-1} K^{-1}
Volumetric heat capacity	ρc	2.5×10^6	J m^{-3} K^{-1}
Thermal diffusivity	α	$0.8–1.0 \times 10^{-6}$	m^2 s^{-1}
Temperature difference	ΔT	80–120	°C
Thermal expansion coefficient	β	3×10^{-4}	K^{-1}
Kinematic viscosity	ν	$3–5 \times 10^{-7}$	m^2 s^{-1}
Gravitational acceleration	g	9.81	m s^{-2}
		Derived dimensionless numbers	
Parameter	Expression	Estimated Range	Interpretation
Peclet number	$Pe = vH/\alpha$	1–15	Weak to moderate advective influence; conduction remains dominant at basin scale
Rayleigh number	$Ra = g\beta\Delta TkH/(\nu\alpha)$	10–500	Below values typically associated with sustained basin-scale free convection
Dominant heat-transfer mode	—	—	Conductive with localized fault-controlled advective enhancement

References

Angelier J. and Baruah S. Seismotectonics in Northeast India: a stress analysis of focal mechanism solutions of earthquakes and its kinematic implications // Geophysical Journal International. — 2009. — Vol. 178, no. 1. — P. 303–326. — https://doi.org/10.1111/j.1365-246x.2009.04107.x

Bhandari L. L., Fuloria R. C. and Sastri V. V. Stratigraphy of Assam Valley, India // AAPG Bulletin. — 1973. — Vol. 57, no. 4. — P. 642–654. — https://doi.org/10.1306/819a4310-16c5-11d7-8645000102c1865d

Bharali B. and Gogoi N. Sand development pattern within the Palaeocene-lower Eocene sediments along the shelf areas of Upper Assam Basin // GEO-India 2011 The 2nd South Asian Geoscience Conference 12–14 January 2011. — AAPG, 2011.

Bhuyan D. Late Eocene unstable basin margin Kopili sedimentation and its reservoir characteristics in upper Assam petroliferous basin // International Journal of Research and Scientific Innovation. — 2016. — Vol. 3, no. 2. — P. 10–15.
Bhuyan D., Borgohain P. and Bezbaruah D. Diagenesis and reservoir quality of Oligocene Barail Group of Upper Assam Shelf, Assam and Assam Arakan basin, India // Journal of Asian Earth Sciences: X. — 2022. — Vol. 7. — P. 100100. — https://doi.org/10.1016/j.jaesx.2022.100100
Bhuyan D. and Dutta I. Paleocene-Eocene Palynostratigraphy of the Northern Margin of Upper Assam Basin, India // International Journal of Geology and Earth Sciences. — 2015. — Vol. 1. — P. 65–80.
Borgohain R., Khound D. J., Bhuyan D., et al. Petrographic study of the Nurpuh sandstone member of a part of Upper Assam Basin // Journal of Earth Sciences. — 1998. — Vol. 1. — P. 29–46.
Crowell A. M. Identifying potential geothermal resources from co-produced fluids using existing data from drilling logs: Williston Basin, North Dakota. — Theses, Dissertations. 12741, 2011.
Dalsania K. P., Sircar A., Pandey V., et al. Prospects of geothermal field development in Gandhar, Gujarat, India // Unconventional Resources. — 2024. — Vol. 4, no. 1. — P. 100093. — https://doi.org/10.1016/j.uncres.2024.100093
Das P. M. A Review of Stratigraphy of parts of Upper Assam Shelf & Mizoram // 4th South Asian Geosciences Conference & Exhibition. — GEO INDIA, 2018.
Deb S. S. and Barua I. Depositional environment, reservoir characteristics and extent of sediments of Langpar & Lakadong+Therria in Chabua area of Upper Assam Basin // 8th Biennial International Conference & Exposition on Petroleum Geophysics. Vol. 177. — 2010.
Devi N. R., Singh Y. R., Abbott M. B., et al. Palynology, palynofacies and organic geochemistry analysis of the late Eocene shale from Meghalaya, Northeast India // Journal of Earth System Science. — 2021. — Vol. 130, no. 2. — https://doi.org/10.1007/s12040-021-01562-w
Dezayes C. and Lerouge C. Reconstructing Paleofluid Circulation at the Hercynian Basement/Mesozoic Sedimentary Cover Interface in the Upper Rhine Graben // Geofluids. — 2019. — Vol. 2019. — P. 1–30. — https://doi.org/10.1155/2019/4849860
DiPippo R. Geothermal power plants: principles, applications, case studies and environmental impact. — Elsevier, 2016. — https://doi.org/10.1016/c2014-0-02885-7
Dutta A. J., Gogoi N., Hussain F. Z., et al. Integrated coupled assessment of geostorage and geothermal prospects in the oil fields of Upper Assam Basin // Scientific Reports. — 2024. — Vol. 14, no. 1. — P. 12390. — https://doi.org/10.1038/s41598-024-60292-3
Faulds J., Hinz N., Coolbaugh M., et al. The Nevada play fairway project – Phase II: Initial search for new viable geothermal systems in the Great Basin region, western USA // GRC Transactions. — 2016. — Vol. 40.
Förster A. and Merriam D. F. A bottom-hole temperature analysis in the American Midcontinent (Kansas): Implications to the applicability of BHTs in geothermal studies // Proceedings of the World Geothermal Congress. Vol. 2. — 1995. — P. 777–782.
Gascuel V., Bédard K., Comeau F. A., et al. Geothermal resource assessment of remote sedimentary basins with sparse data: lessons learned from Anticosti Island, Canada // Geothermal Energy. — 2020. — Vol. 8, no. 1. — https://doi.org/10.1186/s40517-020-0156-1
Gautam T., Sircar A. and Yadav K. Geothermal energy extraction from abandoned well: a roadmap for Cambay Basin // Energy Storage and Saving. — 2025. — Vol. 4, no. 3. — P. 323–341. — https://doi.org/10.1016/j.enss.2025.01.004
Gogoi M. P., Borgohain P., Gogoi Y. K., et al. Petrography, Diagenesis and Hydrocarbon Source Potential of the Barail and Disang Group of Rocks in Parts of the Naga Schuppen Belt and Inner Fold Belt of Assam-Arakan Basin // Journal of the Geological Society of India. — 2023. — Vol. 99, no. 7. — P. 906–916. — https://doi.org/10.1007/s12594-023-2412-z
Hazarika S., Boruah A., Das R., et al. Characterizing Barail shale rock for CO_2 storage potential in the Assam Arakan Basin, India // Petroleum Science and Technology. — 2025. — Vol. 44, no. 2. — P. 163–184. — https://doi.org/10.1080/10916466.2025.2464028
Higgins B. and Pratson L. Repurposing horizontally drilled oil & gas wells for geothermal systems using a coaxial borehole heat exchanger // Energy Conversion and Management. — 2026. — Vol. 348. — P. 120798. — https://doi.org/10.1016/j.enconman.2025.120798
Hochstein M. P., Zheng K., Pasvanoglu S., et al. Advective (heat sweep) geothermal systems // PROCEEDINGS, Thirty-Eighth Workshop on Geothermal Reservoir Engineering. — California, 2013.
Kehle R. O., Schoeppel R. J. and Deford R. K. The AAPG geothermal survey of North America // Geothermics. — 1970. — Vol. 2. — P. 358–367. — https://doi.org/10.1016/0375-6505(70)90034-9
Kiryukhin A. V. High-temperature fluid flows in the Dachny field of the Mutnovsky hydrothermal system, Russia // Geothermics. — 1993. — Vol. 22, no. 1. — P. 49–64. — https://doi.org/10.1016/0375-6505(93)90020-n

Krishnan M. S. Geology of India and Burma. — LBS Publisher, 1960.
Kumar M., Mandal J., Dutta S. K., et al. Palynostratigraphy of the subsurface sediments of Upper Assam Basin, India // Geobios. — 2001. — Vol. 34, no. 3. — P. 241–251. — https://doi.org/10.1016/s0016-6995(01)80072-3
Kumar P. C. and Sain K. Seismic Texture of Tertiary Successions: Insights from Tipam and Barail Formations in the Upper Assam Basin, NE India // Journal of the Geological Society of India. — 2022. — Vol. 98, no. 12. — P. 1671–1679. — https://doi.org/10.1007/s12594-022-2236-2
Lozovsky I., Varentsov I. and Walia D. Crustal and Upper Mantle Structure of the Assam Valley Region, NE India: A Review of Geophysical Findings // Geosciences. — 2025. — Vol. 15, no. 1. — P. 27. — https://doi.org/10.3390/geosciences15010027
Majumdar D. and Devi A. Oilfield geothermal resources of the Upper Assam Petroliferous Basin, NE India // Energy Geoscience. — 2021. — Vol. 2, no. 4. — P. 246–253. — https://doi.org/10.1016/j.engeos.2021.07.002
Meenakshisundaram A., Tomomewo O. S., Aimen L., et al. A comprehensive analysis of repurposing abandoned oil wells for different energy uses: Exploration, applications, and repurposing challenges // Cleaner Engineering and Technology. — 2024. — Vol. 22. — P. 100797. — https://doi.org/10.1016/j.clet.2024.100797
Nandy D. R. Tectonic patterns in northeastern India // Indian Journal of Earth Science. — 1980. — Vol. 7. — P. 103–107.
Nandy D. R. The Eastern Himalayas and the Indo-Burman orogen in relation to the Indian plate movement // Miscellaneous Publication-Geological Survey of India. — 1983. — Vol. 43. — P. 153–159.
Nandy D. R. Geodynamics of Northeastern India and the adjoining region. — Scientific Book Centre, 2017.
Nibbs W., Watson S. M., Kolo I., et al. Repurposing onshore hydrocarbon wells as deep borehole heat exchangers: A comprehensive modelling study for the UK // Applied Thermal Engineering. — 2026. — Vol. 288. — P. 129530. — https://doi.org/10.1016/j.applthermaleng.2025.129530
Nordquist J. and Johnson L. Production of power from the co-produced water of oil wells, 3.5 years of operation // Geothermal Resources Council Transactions. — Geothermal Resources Council 2012 Annual Meeting, 2012. — P. 207–210.
Ojaghi H., Shahin M., Simjoo M., et al. Repurposing abandoned oil and gas wells for geothermal energy extraction: A review of concepts, challenges, and opportunities // Applied Energy. — 2025. — Vol. 401. — P. 126816. — https://doi.org/10.1016/j.apenergy.2025.126816
Prater M. L., Cheung P. K., Luza K. V., et al. Geothermal resource assessment in Oklahoma. — Oklahoma Geological Survey, The University of Oklahoma, 1981.
Quoilin S., Van Den Broek M., Declaye S., et al. Techno-economic survey of Organic Rankine Cycle (ORC) systems // Renewable and Sustainable Energy Reviews. — 2013. — Vol. 22. — P. 168–186. — https://doi.org/10.1016/j.rser.2013.01.028
Sarolkar P. B. Geothermal energy in India: poised for development // PROCEEDINGS, 43rd Workshop on Geothermal Reservoir Engineering. — California, 2018.
Simmons S. F., Kirby S., Verplanck P., et al. Strategic and critical elements in produced geothermal fluids from Nevada and Utah // PROCEEDINGS, 43rd Workshop on Geothermal Reservoir Engineering. — California, 2018. — P. 12–14.
Taye C. and Bhattacharyya P. Petrographic Characteristics of Basement Rocks in A few Bore Holes of Upper Assam Basin // Geology. — 2013. — Vol. 2, no. 2.
Tiwari A., Memory S. L., Joseph J., et al. Mineralogical and geochemical studies of shales from Kopili Formation, Dima Hasao district Assam, North East India: Insights into diagenesis, deposition and provenance // Evolving Earth. — 2024. — Vol. 2. — P. 100039. — https://doi.org/10.1016/j.eve.2024.100039
Wandrey C. J. Sylhet-Kopili/Barail-Tipam Composite Total Petroleum System, Assam Geologic Province, India. — USGS Publications Warehouse, 2004. — https://doi.org/10.3133/b2208d
Waples D. W. and Ramly M. A statistical method for correcting log-derived temperatures // Petroleum Geoscience. — 2001. — Vol. 7, no. 3. — P. 231–240. — https://doi.org/10.1144/petgeo.7.3.231
Xin S., Liang H., Hu B., et al. Electrical Power Generation from Low Temperature Co-Produced Geothermal Resources at Huabei Oilfield // ROCEEDINGS, Thirty-Seventh Workshop on Geothermal Reservoir Engineering. — California, 2012.
Ye X., Yu Z., Zhang Y., et al. Mineral Composition Impact on the Thermal Conductivity of Granites Based on Geothermal Field Experiments in the Songliao and Gonghe Basins, China // Minerals. — 2022. — Vol. 12, no. 2. — P. 247. — https://doi.org/10.3390/min12020247